Geosci. Model Dev. Discuss., 2, 209–246, 2009
www.geosci-model-dev-discuss.net/2/209/2009/

Geoscientific Model Development Discussions

Geoscientific Model Development Discussions is the access reviewed discussion forum of *Geoscientific Model Development*

Aerosol microphysics modules in the framework of the ECHAM5 climate model – intercomparison under stratospheric conditions

H. Kokkola[1,2], R. Hommel[1,4], J. Kazil[1], U. Niemeier[1], A.-I. Partanen[1,3,5], J. Feichter[1], and C. Timmreck[1]

[1]Max Planck Institute for Meteorology, Hamburg, Germany
[2]Finnish Meteorological Institute, Kuopio, Finland
[3]Tampere University of Technology, Tampere, Finland
[4]Centre for Atmospheric Science, Cambridge Univ., Department of Chemistry, Cambridge, UK
[5]University of Kuopio, Department of Physics, Finland

Received: 26 February 2009 – Accepted: 26 February 2009 – Published: 9 March 2009

Correspondence to: H. Kokkola (harri.kokkola@fmi.fi)

Published by Copernicus Publications on behalf of the European Geosciences Union.

Abstract

In this manuscript, we present an intercomparison of three different aerosol microphysics modules that are implemented in the climate model ECHAM5. The comparison was done between the modal aerosol microphysics module M7, which is currently the default aerosol microphysical core in ECHAM5, and two sectional aerosol microphysics modules SALSA, and SAM2. A detailed aerosol microphycical model MAIA was used as a reference model to evaluate the results of the aerosol microphysics modules with respect to sulphate aerosol.

The ability of the modules to describe the development of the aerosol size distribution was tested in a zero dimensional framework. We evaluated the strengths and weaknesses of different approaches under different types of stratospheric conditions. Also, we present an improved method for the time integration in M7 and study how the setup of the modal approach affects the evolution of the aerosol size distribution.

Intercomparison simulations were carried out with varying SO_2 concentrations from background conditions to extreme values arising from stratospheric injections of large volcanic eruptions. Under background conditions, all microphysics modules were in good agreement describing the shape of the size distribution but the scatter between the model results increased with increasing SO_2 concentrations. In particular for the volcanic case the module setups have to be redefined to be applied in global model simulations capturing respective sulphate particle formation events.

Summarized, this intercomparison serves as a review on the different aerosol microphysics modules which are currently available for the climate model ECHAM5.

1 Introduction

While greenhouse gases such as carbon dioxide and methane have been shown to have a large effect on climate by warming the Earth's surface when absorbing the long wave radiation emitted from earth (e.g. Fleming, 1998; Le Treut et al., 2007; Weart,

GMDD

2, 209–246, 2009

2003), it has been acknowledged that increased atmospheric concentrations of aerosol particles might drive a significant radiative forcing process of the planet (Twomey, 1974; Seinfeld and Pandis, 1998; IPCC, 2007). The knowledge of the impacts of aerosols on health, atmospheric composition and climate is still incomplete. Even more uncertainties lie in the understanding of direct and indirect effects of aerosols on climate and how these effects are modified by aerosol processing and aerosol composition (Chen and Penner, 2005).

To comprehensively assess the impact of aerosol particles on ozone concentration, cloud formation and radiative forcing, information about the particle size and number density is necessary (e.g. Zhang et al., 2002; Dusek et al., 2006). In global scale atmospheric models, modeling aerosol processes is always a compromise between accuracy and computational efficiency. Thus the descriptions of the aerosol size as well as the chemical composition of aerosol populations have to be simplified. The aerosol distribution in aerosol modules is described in most cases done using bulk approach (Liao and Seinfeld, 2005; Liu et al., 2005; Reddy et al., 2005; Rasch et al., 2008), modal approach (Ghan et al., 2001; Wilson et al., 2001; Vignati et al., 2004; Lauer et al., 2005; Stier et al., 2005), and sectional approach (Jacobson, 2001; Timmreck, 2001; Rodriguez and Dabdub, 2004; Spracklen et al., 2005; Hommel, 2008; Kokkola et al., 2008). In the bulk approach, only the aerosol mass is prognostic. The particle sizes can then be retrieved assuming e.g. monodisperse or prescribed size distributions. The bulk approach is computationally very efficient, but introduces a large error when calculating strongly size dependent physical effects of aerosols, such as scattering of radiation and cloud activation (e.g. Zhang et al., 2002). While in the mono-disperse approach a particle population is assumed to be of uniform size, both modal and sectional aerosol schemes resolve entire particle spectra and are able to consider more than a single aerosol moment. Several model studies highlight the importance of a simultaneous prognostic treatment of both aerosol mass and number for aerosol-climate process interactions (e.g. Adams and Seinfeld, 2002). Depending on the number of aerosol species treated by the aerosol modules, the modal approach is computation-

ally preferable than the sectional approach, since the computer capacity consumption of the latter in global climate simulations can easily exceed today's available high performance computing facilities (e.g. Ghan and Schwartz, 2007). Nevertheless, simplifying the aerosol size distribution by the assumption of log-normal modes is a source of uncertainty when the shape of the size distribution is heavily modified by microphysical processes. This can be crucial especially in studies of evolving perturbations of the stratospheric aerosol layer since the mean aerosol life time there can achieve several years, compared to a few days under tropospheric conditions (e.g. WMO/SPARC, 2006).

Under stratospheric background conditions, concentrations of sulphate aerosol precursor gases remain relatively low (WMO/SPARC, 2006), thus the size and number spectra of respective liquid sulphate particles formed from oxidation of those gases above the tropopause are characterized by mean radii at least a magnitude smaller than under volcanically perturbed conditions (e.g. Brock et al., 1993; WMO/SPARC, 2006). In parametrization of aerosol-climate interactions a specific aerosol parameter is of special interest: The area weighted mean radius, or effective radius (R_{eff}), which characterizes aerosol populations independent of the shape of their distribution. From multi-instrument analysis Russell et al. (1996) derived a typical effective radius of stratospheric background aerosol with 0.17±0.07 µm. After volcanic eruptions when sulphur species concentrations are increased drastically, the particles grow larger and the stratospheric aerosol size distribution is significantly altered for a couple of years. One year after the 1991 Mt. Pinatubo eruption an increase in the effective radius of up to 0.5 µm has been observed which is then slowly declining with an folding time of four years (WMO/SPARC, 2006). Recently, an enhanced stratospheric aerosol load in conjugation with modulated particle size properties have also become of increasing scientific interest in the light of geoengineering the climate using human-induced artificial sulphate aerosol (e.g. Crutzen, 2006; Rasch et al., 2008).

The size distribution of aerosol populations has a strong influence on climate, as larger particles scatter less visible light than smaller particles and, in the case of non-

sulphate or mixed phase aerosol, absorb more efficiently in the near- and far-infrared. It is therefore important to asses the abilities of different microphysical approaches to simulate the temporal development of particle size distributions under evolving atmospheric conditions (volcanoes, geoengeering). In the following we will focus on initial changes in the stratospheric sulphate aerosol distribution after a volcanic eruption encompassing small and large (Mt. Pinatubo size) SO_2 emissions.

In Sect. 2 principal features of the aerosol microphysics modules participating in this inter-comparison are introduced. Followed by a detailed description of the improved time integration scheme for M7 in Sect. 3, completed by validation against the variable-coefficient ordinary differential equation solver (VODE). In Sect. 4, the experimental conditions are described. In Sect. 5, different treatments of resolving the aerosol spectra in M7 are compared and the simulated number distributions of all participating aerosol modules under stratospheric conditions, varying the initial SO_2 concentration from typical background to assumed volcanic conditions are investigated. Finally, the respective effective radii are derived and compared for an ensemble of ten day simulations. A summary can be found in Sect. 6.

2 Aerosol microphysics modules

In this intercomparison, we compare four different aerosol microphysics modules MAIA, SAM2, SALSA, and M7. Of these, MAIA and SAM2 treat sulphate as the sole aerosol chemical component while SALSA and M7 include also organic compounds, sea salt, black carbon, and mineral dust. The modules describe the processing of aerosol size distribution through the following microphysical processes:

- New particle formation by nucleation.
- Condensation of gas phase compounds to the particle phase.
- Coagulation of the aerosol particles.

– Thermodynamical equilibrium between liquid water and water vapour.

Table 1 summarizes the major features of the aerosol microphysics modules. Three modules of this intercomparison, M7, SALSA, and SAM2 have been designed to be used in large scale climate models and have all been implemented in the climate model ECHAM5 (Roeckner et al., 2003). Since these microphysics modules have been designed for large scale models, they parameterize aerosol microphysical processes and use assumptions to resolve the aerosol size distribution. Binary homogeneous nucleation of sulphate aerosols is treated identically in all the three modules using nucleation scheme by Vehkamäki et al. (2002) extending it for high concentrations of sulphate using collision rate as nucleation rate (H. Vehkamäki, personal communication). For other microphysical processes the treatment varies between the modules. To evaluate the results of these modules, the aerosol module MAIA was considered as a reference since it has a highly resolved particle size spectrum and it is based on advanced numerical, thermodynamical and kinetic approaches compared to parameterizations which are currently used in aerosol modules suitable for global climate simulations.

Even though the microphysics modules all solve the same microphysical processes, the methods used in the modules vary significantly. Following is a brief description of formulation of the microphysics modules including improvements introduced in the modules in this study.

2.1 MAIA

The reference model in this study is a detailed aerosol model MAIA (Model of Aerosols and Ions in the Atmosphere) (Lovejoy et al., 2004; Kazil et al., 2007). MAIA simulates microphysical processes of neutral and charged (negative) H_2SO_4/H_2O aerosol particles. The aerosol size distribution is represented with a hybrid kinetic-sectional scheme: In the kinetic part, the model resolves the concentrations of aerosol particles containing up to 21 H_2SO_4 molecules individually. For larger particles, the model uses geometric size sections. The size distribution within these geometric size sections is

resolved with linear functions. This approach suppresses numerical diffusion better than a doubling of the number of size sections at a negligible computational expense. The system of differential equations for the particle concentrations in the model size sections is integrated with the VODE solver (Brown et al., 1989).

MAIA describes nucleation and growth of small neutral and charged molecular clusters based on laboratory thermochemical data (Curtius et al., 2001; Lovejoy and Curtius, 2001; Froyd and Lovejoy, 2003a,b; Hanson and Lovejoy, 2006). The thermochemical data for H_2SO_4/H_2O uptake and loss by large aerosol particles derive from the liquid drop model and H_2SO_4 and H_2O vapor pressures over bulk solutions, calculated with a computer code (Clegg, S. L., personal communication, 2007.) that uses data from Giauque et al. (1960) and Clegg et al. (1994).

The thermodynamic data for intermediate sized particles are a smooth interpolation of the data for the small and large particles. The rate coefficients for sulphuric acid uptake and loss by the aerosol particles, for the coagulation of the aerosol particles, and for the recombination of the negatively charged aerosol with cations are calculated with the Fuchs formula for Brownian coagulation (Fuchs, 1964) and averaged over the equilibrium H_2O content probability distribution of the aerosol. This simplification holds well in the troposphere, where water is more abundant by orders of magnitude than sulphuric acid, so that the aerosol particles have ample time to equilibrate with respect to water uptake/loss before colliding with a H_2SO_4 molecule.

2.2 M7

M7 (Vignati et al., 2004) is the microphysical core of aerosol module HAM (Stier et al., 2005) of ECHAM5. The aerosol microphysics module M7 describes the aerosol size-distribution by 7 log-normal modes, predicting the mode size, mixing state, and composition. In the default setup of M7, the modes are assumed to have a fixed geometric standard deviation σ_g of 2.0 for coarse modes and 1.59 for finer modes, so the size distribution can be described by mode radius R_p, number concentration and composition and thus less variables are needed to describe the particle size interval compared

to a sectional model. This makes M7 computationally very efficient.

The aerosol population is divided into two types of particles: mixed, or water-soluble particles, and insoluble particles. Soluble aerosols are assumed to exist in nucleation mode (R_p<0.005 µm), Aitken mode (0.005 µm<R_p<0.05 µm), accumulation mode (0.05 µm<R_p<0.5 µm), and coarse mode (R_p>0.5 µm), while insoluble aerosols are assumed to exist in Aitken, accumulation, and coarse mode. However, since in this intercomparison, only sulphate is treated, the insoluble modes are not used in the simulations.

Previously, M7 has integrated the differential equation for the aerosol compounds using a computationally efficient operator splitting scheme (Vignati et al., 2004). However, this approach may cause significant numerical diffusion when time steps typical for global scale models are used. An improved time integration scheme for M7 is described in Sect. 3.

2.3 SALSA

SALSA follows the formulation of M7 using sectional approach as opposed to the modal approach of M7. The size sections have been divided in three subranges that have different degree of external mixing, width of the size section, and number of chemical compounds. Particle diameters in subranges, and their chemical composition are defined as follows: Subrange 1: particles with diameter D_p<0.05 µm, Subrange 2: 0.050 µm≤D_p<0.73 µm, and Subrange 3: D_p≥0.73 µm.

- Subrange 1: three internally mixed size sections consisting of sulphate and organic carbon. Sizes are calculated using the moving center method (Jacobson, 2005).

- Subrange 2: four externally mixed size sections – soluble and insoluble – per size section consisting of sulphate, organic carbon, sea salt, black carbon and mineral dust. Sizes are calculated using the moving center method.

– Subrange 3: three externally mixed size sections – insoluble, cloud activating insoluble, and soluble – consisting of sulphate, organic carbon, sea salt, black carbon and mineral dust. Sizes in the subrange 3 are calculated using the fixed center method, since the sizes of these particles are not assumed to be sensitive to microphysical processing in most atmospheric conditions.

Since in this intercomparison, sulphate is considered as the sole chemical component in the aerosol particles, the insoluble size sections are not used in this intercomparison reducing the number of size sections to 10. When also insoluble size sections are in use, the number of size sections in SALSA is 20.

For nucleation, SALSA applies the parameterization by Kerminen and Kulmala (2002), which determines the formation rate of 3 nm particles from the nucleation rate given by the Vehkamäki et al. (2002) scheme. Condensation of gas phase compounds onto the particles is calculated concurrently with nucleation using the analytical predictor of nucleation and condensation method (Jacobson, 2005). Coagulation is calculated using a semi-implicit method (Jacobson, 1994).

For a more detailed description of the structure and methods used in SALSA, see Kokkola et al. (2008).

2.4 SAM2

SAM2 is a one moment aerosol scheme treating the aerosol mass in each bin prognostically. The scheme follows the fixed sectional approach (Gelbard et al., 1980) to resolve an aerosol distribution from 1×10^{-3} µm to 20.64 µm in radius. 44 logarithmically spaced size bins are determined by mass doubling.

Unlike M7 and SALSA, which assume zero saturation vapor pressure of H_2SO_4 at the particle surface, SAM2 is able to treat the mass transfer of sulphuric acid vapor reversely without further parameterizations for evaporating particles. Considering the latter process is of relevance for global aerosol-climate models designated for investigations of volcanic effects on stratospheric aerosol, since evaporation determines the

vertical limitation of the global dispersion of liquid aerosol particles in regions where the stratosphere is locally subsaturated with respect to their vapor concentrations (Hamill et al., 1977). In SAM2 the change in the aerosol size distribution due to reversible gas-to-particle partitioning of H_2SO_4 is treated as an advective type process that allows particles to grow and shrink virtually in radius space. Here a one-dimensional hybrid exponential-upwind advection scheme (Spalding, 1972; Chlond, 1994; Timmreck and Graf, 2000) ensures the preservation of the particle number concentration under conditions of the "whole atmosphere". This is of special interest when an aerosol distribution is characterized by steep gradients, which will be shaped e.g. when ultrafine aerosols nucleate from the gas phase.

Brownian coagulation is considered following a semi-implicite mass conserving formulation by Timmreck and Graf (2000). As opposed to the time integration scheme of SALSA and the new time integration scheme of M7, the time integration of individual microphysical processes in SAM2 is processed sequentially. A complete description of the parameterizations implemented in SAM2 and its overall performance in the context of a global aerosol-climate model resolving the troposphere and the stratosphere up to ~80 km can be found in Hommel (2008).

3 New time integration scheme of H_2SO_4 processes in M7

A new method for the integration of the time evolution equation

$$\frac{d[H_2SO_4]}{dt} = P - L \cdot [H_2SO_4] - R([H_2SO_4]) \quad (1)$$

for the concentration of gas phase sulphuric acid has been implemented in the M7 aerosol microphysics module. P denotes the production rate of gas phase H_2SO_4, L its loss rate due to condensation onto aerosol particles, $R([H_2SO_4])$ the removal rate of gas phase sulphuric acid due to aerosol nucleation, and t the time. P and L depend on gas and aqueous phase chemistry and aerosol microphysics, and are determined in

separate time integration (operator splitting) procedures before or after the integration of Eq. (1). They are considered constant for the integration of Eq. (1) over one time step.

In the Euler backward scheme, Eq. (1) is discretized as

$$\frac{[H_2SO_4]_{t+\Delta t} - [H_2SO_4]_t}{\Delta t} = P - L \cdot [H_2SO_4]_{t+\Delta t} - R([H_2SO_4]_{t+\Delta t}) \quad (2)$$

which can be rewritten to

$$[H_2SO_4]_{t+\Delta t} = \frac{[H_2SO_4]_t + \Delta t P - \Delta t R([H_2SO_4]_{t+\Delta t})}{1 + \Delta t L}. \quad (3)$$

This equation is then solved for $[H_2SO_4]_{t+\Delta t}$, typically iteratively. However, the iteration and a repeated evaluation of the removal rate R until a satisfactory degree of convergence is achieved may not to be computationally affordable. A common approach is then to abort the iteration after all processes have been calculated once. This can be realized with operator splitting between production/loss and nucleation: When the iteration is initialized as

$$\begin{aligned} [H_2SO_4]^0_{t+\Delta t} &= \frac{[H_2SO_4]_t + \Delta t P}{1 + \Delta t L} \\ [H_2SO_4]^1_{t+\Delta t} &= \frac{[H_2SO_4]_t + \Delta t P - \Delta t R([H_2SO_4]^0_{t+\Delta t})}{1 + \Delta t L} \\ &\vdots \end{aligned} \quad (4)$$

then the first two steps can be interpreted as

$$[H_2SO_4]^{PL}_{t+\Delta t} = \frac{[H_2SO_4]_t + \Delta t P}{1 + \Delta t L} \quad (5)$$

GMDD
2, 209–246, 2009

$$[H_2SO_4]^{PLN}_{t+\Delta t} = [H_2SO_4]^{PL}_{t+\Delta t} - \frac{\Delta t R([H_2SO_4]^{PL}_{t+\Delta t})}{1 + \Delta t L} \quad (6)$$

which corresponds to calculating the concentration of gas phase H_2SO_4 after production and loss (PL) and then after nucleation (PLN). However, $[H_2SO_4]^{PL}_{t+\Delta t}$ in Eq. (5) can be computed exactly by exploiting the fact that if nucleation is neglected, Eq. (1) has an analytical solution:

$$[H_2SO_4](t) = \left([H_2SO_4](t_0) - \frac{P}{L}\right) \cdot e^{-L(t-t_0)} + \frac{P}{L}. \quad (7)$$

The new integration method therefore reads

$$[H_2SO_4]^{PL}_{t+\Delta t} = ([H_2SO_4]_t - \frac{P}{L}) \cdot e^{-L\Delta t} + \frac{P}{L} \quad (8)$$

$$[H_2SO_4]^{PLN}_{t+\Delta t} = [H_2SO_4]^{PL}_{t+\Delta t} - \frac{\Delta t R([H_2SO_4]^{PL}_{t+\Delta t})}{1 + \Delta t L}$$

Unlike the Euler backward scheme and the original M7 time integration method, the new time integration has the advantage to converge towards the exact solution of Eq. (1) for all time step lengths with decreasing nucleation ($R \rightarrow 0$). As in the original M7 time integration, a safeguard is implemented which prevents the gas phase sulphuric acid concentration from becoming negative: When the removal due to nucleation in the course of a time step would exceed the initially available and newly produced gas phase sulphuric acid, all of it is converted to newly formed particles, and its concentration is set to zero.

3.1 Verification of the new time integration scheme

The performance of the new time integration scheme was tested against the Euler backward scheme, the original M7 time integration method, and the VODE solver

(Brown et al., 1989) which uses the variable coefficient Adams-Moulton method for non-stiff ordinary differential equations and time step lengths based on a desired relative error tolerance.

Three different cases were considered, with ambient conditions chosen so that H_2SO_4 decreases, is kept constant, or increases. The conditions for the three cases are given in Table 2. The same pressure (1013.25 hPa), ion pair production rate ($4\,cm^{-3}s^{-1}$), diameter of the preexisting aerosol particles (0.165 µm), and mass density of the preexisting aerosol particles ($2\,g\,cm^{-3}$) was used in all three cases. Nucleation rates and the resulting removal rates of gas phase sulphuric acid were calculated with the method of Kazil and Lovejoy (2007).

Figure 1 shows the gas phase sulphuric acid concentration after one time step, as a function of the time step length, calculated with the new time integration method, the Euler backward scheme, and the original M7 method. As a reference, the gas phase sulphuric acid concentration calculated with the VODE solver is given, which divides the time step into shorter integration steps, based on a desired relative error tolerance (10^{-9} in this comparison).

In cases 1 and 3 the new time integration method performs as well as VODE and better than the Euler backward scheme. In case 2 the new time integration method and the Euler backward scheme produce very similar results (overlapping curves), both underestimating the sulphuric acid concentration obtained with the VODE solver. The systematic bias is increasing with increasing time step length. In contrast, the original M7 method significantly underestimates sulphuric acid gas phase concentrations in all three cases, and predicts a total removal of the available sulphuric acid in the gas phase at longer time step lengths in the cases 1 and 3. The underestimation of the gas phase concentrations for shorter time step lengths arises from an overestimation of condensation by this scheme. The zero values in cases 1 and 3 for longer time steps result from an overestimation of the loss of sulphuric acid via nucleation, which exceeds the available gas phase sulphuric acid, and which is entirely converted to new particles. A complete conversion of the available gas phase sulphuric acid to new

GMDD
2, 209–246, 2009

particles can also result with the new time integration method and the Euler backward scheme, but requires higher nucleation rates or longer time steps compared with the original M7 method.

Overall, the new time integration method outperforms both the original M7 method and the Euler backward scheme for the solution of the gas phase sulphuric acid time evolution equation with concurrent nucleation and condensation. In the following simulations, we have used this new time integration method.

4 Experimental setup

The ability of the microphysics modules to describe the processing of the sulphate aerosol size distribution was investigated by calculating the evolution of the size distribution over a 10 day period assuming typical conditions of the midlatitude stratosphere at 30 hPa ambient pressure and 214.8 K temperature. Initial stratospheric sulphate size distribution was assumed to be unimodal with 0.234 µm geometric mean diameter, 1.59 geometric standard deviation, and a total number concentration of 3 cm^{-3}.

The evolution of the size distribution was affected by varying the initial SO_2 concentration which modifies the size distribution through oxidation to H_2SO_4 and subsequent gas-to-particle partitioning processes. We assume that gaseous H_2SO_4 is exclusively formed from the oxidation of SO_2 by the hydroxyl radical OH. The concentration of the latter is prescribed by an abstracted diurnal cycle with a daytime concentration of 1×10^6 cm^{-3} between 06:00 and 18:00. This value was derived from a time slice experiment conducted with the chemistry-climate model MAECHAM4-CHEM (Timmreck et al., 2003). The initial SO_2 mixing ratio was varied between a typical background value of 1.5×10^{-11} kg/kg (~10 pptv; WMO/SPARC, 2006) and 3.9×10^{-4} kg/kg for the assumed volcanic case and two intermediate mixing ratios of 3.9×10^{-8} kg/kg and 3.9×10^{-6} kg/kg. The extreme case mixing ratio was derived from a 3-D simulation of the Mt. Pinatubo episode with use of the model MAECHAM5 (Niemeier et al., paper in preparation, 2009), initializing 17 Mt SO_2 (Read et al., 1993). The sensitivity studies

presented in the following were conducted using integration time step length of Δt= 1 s, 60 s, and 900 s was investigated. The latter corresponds to the default time step of ECHAM5 using the spectral truncation T42.

In M7, the standard deviation σ_g of the individual modes is fixed, so the choice of the value for σ_g affects the module's ability to describe the development of the size distribution especially in conditions, where the shape of the size distribution is heavily modified, for example when high concentrations of sulphuric acid vapor yield to high mass transfer rates into the particle phase. The role of the coarse mode in M7 is to describe primary sea salt and dust particles which are mainly present in the troposphere. Sulphate aerosol can be sufficiently prescribed with three modes as already shown in the M3 model (Wilson and Raes, 1996; Wilson et al., 2001), a predecessor model of M7. Therefore we tested two different mode setups in M7, the default mode setup and a second setup in which the coarse mode was neglected.

- Setup 1, default size distribution of M7; σ_g=1.59 for nucleation, aitken and accumulation mode, σ_g=2.00 for coarse mode.
- Setup 2, σ_g=1.59 for nucleation, aitken and accumulation mode, no coarse mode.

5 Results and discussion

5.1 Size distributions

First, we compared the shapes of aerosol size distributions calculated by individual aerosol microphysics modules when the size distribution is modified by gas-to-particle conversion of sulphur.

In Fig. 2, the number size distributions at 12:00, 10 days into the simulations are shown for the given different initial gas phase mixing ratios and different time step lengths. Each row in Fig. 2 represents a simulation using a specific initial mixing of

SO_2 and the columns represent the time step length. The mixing ratios and time step lengths are denoted in the title of each subplot.

From Fig. 2, we can see that all microphysics modules reproduce the shape of the size distribution given by the reference model well for background conditions and also when the SO_2 load was moderately enhanced (two upper rows). Also in these cases, the time step length has no significant effect on the final size distribution.

As the initial SO_2 mixing ratio is increased, the calculated size distributions begin to differ for the individual microphysics modules (two lowest rows). Increased SO_2 mixing ratios yield to a separation of the aerosol size distributions into two narrow modes in the ultrafine regime of the size spectrum and the coarse mode respectively. The feature is pronounced for the case representing conditions in the stratosphere in the course of a large volcanic eruption. Although no direct particle number concentration measurements are known to have been carried out immediately after respective volcanic eruptions in regions were the material was injected into the stratosphere, there is evidence from in situ observations that clearly separated bi-modal particle spectra will evolve under conditions as assumed in this study. Brock et al. (1993) reported aircraft measurements in the subtropical northern hemisphere, starting 10 weeks after the eruption of Mt. Pinatubo in 1991. During the first days of the campaign particle size spectrometers registered not continuously but in more than 1/3 of all measurements bi-modal size spectra where a distinct and clearly separated coarse mode appeared beyond particles sizes of 1 µm in diameter. Since the flights were carried out in heights below 40 hPa the authors conclude to measure "fallout" from higher elevations. Due to the fact that these spectrometers were calibrated for sulphuric acid only and volcanic ash fallout terminates after a couple days after it was injected into the stratosphere (Guo et al., 2004), it can be assumed that these ultra large particles contain mainly sulphuric acid.

As can be seen from Fig. 2, when the SO_2 mixing ratio is above background levels, M7 with a fixed standard deviation cannot reproduce the shape of the size distribution at the upper end of the spectrum. The sectional approach has advantages to

reproduce the narrow band structure of the size distribution in the coarse mode nearly independent on the number of sections used to discretise the aerosol spectrum. Under assumed volcanic conditions the default mode setup of M7 also fails to reproduce the distinct bimodal characteristic of the size distribution in particular when the global model time step length of 900 s is used.

In SALSA, to minimize the amount of tracers, only the number concentration is calculated for the size sections in subregion 3. Also, no coagulation between the particles in subregion 3 is assumed, so these size sections are treated as a sink for smaller particles and condensating gases. In normal atmospheric conditions this assumption is valid, but it fails in the volcanic case. This is more evident in the effective radius as will be shown later in Sect. 5.3.

The sensitivity of the modules to the integration time step length increases as the initial SO_2 mixing ratio increases. Because the evolution of the size distribution become more rapid yielding to steeper gradients in the aerosol concentrations. For example for 3.9×10^{-4} kg/kg, SAM2 describes extremely well the final size distribution when time step length of 1 s is used, whereas for Δt of 60 and 900 s a detached bimodal distribution does not appear at the end of the simulation. The evolution of the size distributions as predicted by M7 and SALSA is less affected by the integration time increment. Notable effects are seen here for fine particles and, in particular for M7 setup 1, also for medium size particles.

5.2 M7 with different mode setups

As seen in Fig. 2, high concentrations of SO_2 separated the size distribution in two narrow modes. These cannot be reproduced by M7 setups 1 and 2. Therefore, we introduce a third mode setup to get a better agreement for the simulations with high concentrations of SO_2. The third mode setup is as follows:

- Setup 3, σ_g=1.59 for nucleation and aitken mode, σ_g=1.2 for accumulation mode, no coarse mode.

Here we look in detail to the results for the results given by M7 using the three mode setups described above. Figure 3 shows the aerosol number size distributions at 12:00, 10 days into the simulation compared to the results calculated by the reference model MAIA (red curve). Simulations with M7 were done using time step of 60 s. The magenta curves are calculated using the default size distribution of M7 (setup 1), the green curves are for the mode setup 2, and the blue dashed curves are for mode setup 3.

Figure 3a represents simulations for the background value of SO_2. It can be seen that the reference size distribution given by MAIA is well reproduced by the mode setups 1 and 2. This is because the size distribution is only slightly modified by the small concentrations of sulphate produced from SO_2 oxidation. As expected, under these conditions M7 setup 3 with σ_g=1.2 for the coarse mode is not able to reproduce the shape of the size distribution.

In Fig. 3b, the initial SO_2 mixing ratio is set to an intermediate value of 3.9×10^{-8} kg/kg and the processing of the size distribution by sulphuric acid formed in the gas phase becomes more visible than in Fig. 3a. In this simulation, MAIA clearly predicts a multi-modal distribution which arises from evolving nucleation bursts through particle growth. MAIA predicts a well-established narrow peak at approximately 0.15 µm on top of the accumulation mode. Even though this peak cannot be reproduced by the M7 setups 1 and 2, their curves follow relatively well the size distribution calculated using the reference model. M7 in setup 3 reproduces best the size distribution for the fine modes, but the number concentration at the upper end of the size spectrum is underestimated.

Figure 3c is a simulation under conditions of an assumed volcanic eruption resulting in mixing ratio of 3.9×10^{-4} kg/kg SO_2. As seen before, in this simulation, the size distribution is divided into two separate narrow modes of nucleating particles and coarse particles grown by coagulation and condensation of sulphuric acid.

A distinct coarse mode formed by sulphate particles in the size range between 1 and 10 µm in diameter even after relatively short time scales. The predicted standard deviation of such a mode varies in particular depending on geometric specifications of

the models, as shown in Fig. 3c.

From Fig. 3c we can see that the default mode setup of M7 (setup 1) overestimates the size distribution at the upper end of the spectrum with a coarse mode of σ_g=2.0 appearing. Overestimation of large particles in this setup will probably affect the removal of particles in a volcanic plume and potentially has implications in radiative transfer calculations and respective climate responses. With MAIA as reference, M7 in the mode setup 3 gives the best fit for size distributions under assumed high stratospheric concentrations of SO_2 while the mode setup 2 falls in between the results given by setups 1 and 3.

5.3 Effective radius

Since the shape of the aerosol size distribution affects specific aerosol parameters which are relevant to several aerosol-climate interactions (e.g. Dusek et al., 2006), we derived the effective radius, a key variable that is used in radiative transfer calculations.

Figure 4 is structured as follows: the rows represent the evolution of the effective radii as predicted by the aerosol modules for three different initial SO_2 mixing ratios, whereas the columns represent the parameter derived from specific integration ranges. In the left column of Fig. 4, the effective radii were derived for the whole size range of particles as treated in the modules. Nevertheless, the effective radius from global model results is often compared to respective data retrieved from optical remote sensing technologies (e.g. satellite instruments, Lidar). With respect to water soluble aerosols, the measurement uncertainties of those retrievals raise exponentially for particles with radius below 0.1 µm (e.g. Dubovik et al., 2000; Thomason et al., 2008), that we believe the derived parameters of our model simulations are better represented when the integration of the effective radius is adapted for the "visible" size range of such remote sensing instruments. Therefore, in the right column of Fig. 4 the model results were filtered to represent the particle size above a threshold size of radius $R \geq 0.05$ µm. For all integrations shown in Fig. 4 a time step length of 900 s was used, which is normally applied when the modules are integrated coupled to the global climate model

ECHAM5.

The initial mixing ratios shown here range from slightly and moderately increased stratospheric SO_2 abundances of 3.9×10^{-8} kg/kg in the upper row, and 3.9×10^{-6} kg/kg in the middle row. The bottom panels show how the effective radii are predicted under assumed volcanic conditions with SO_2=3.9×10^{-4} kg/kg.

5.3.1 General behaviour

Before we discuss the module performance for specific SO_2 initial concentrations, the general behavior in predicting the effective radius shall be analyzed. Even though, in Fig. 2 the aerosol number distributions given by different aerosol modules appear very similar in a moderately increased stratospheric concentrations of SO_2, Fig. 4 reveals significant relative differences in the evolution of the effective radii given by the different modules. Under all conditions a steep gradient appears in the evolution of the effective radius in the very first model time steps.

All modules rapidly drift towards a more or less similar state and predict size distributions whose effective radii are smaller by a factor of 2 to 3 than those of the respective initial size distributions, which we assume to represent a typical stratospheric background state in which ultrafine particles were not considered. This drop in R_{eff} results from the formation of particles in the nucleation size range, which are a consequence of SO_2 oxidation when we prescribe the availability of OH during daylight after 6 h of simulation. After dropping to a certain value, the effective radii increase due to further mass transfer of sulphur from the gas to the particle phase which evolve the aerosol distributions towards the coarse mode. The aerosol mass in the modules constantly increases since we neglect the non-microphysical particle sink terms in this experiments. During night, when new particle formation is inhibited, the effective radii increase sharply due to the absence of a nucleation burst and the rapid growing of ultrafine particles. Then further condensation of H_2SO_4 constantly depletes its gas phase reservoir and the mass transfer rate is smaller during night than during day when the availability of OH leads to gaseous sulphuric acid production. Consequently, the rates of change in

evolving R_{eff} are smaller during night.

Our investigations revealed that the magnitude of the diurnal cycle in R_{eff} is related to the shape of the modeled size distribution and depends on module specific definitions. Assuming that MAIA tends to represent the nature of an evolving aerosol effective radius, in the sectional modules SAM2 and SALSA the diurnal cycle in the evolution of R_{eff} amplifies when the stratospheric SO_2 load is increased. On the contrary in the modal module M7 R_{eff} evolves relatively smooth. The predicted size distribution in M7 is less affected by fluctuations in the Aitken mode between day and night, because standard deviations σ_g of the individual modes are predefined and cannot vary: In M7 the condensational flux is partitioned quasi over four bands representing the aerosol size distribution (for the calculation of the flux only the median radii of the modes are of interest). When during night, the nucleation mode particle concentration tends to zero, the available gas is transferred to higher modes only. This yields to a slightly increasing median radius in each mode, not affecting the width of their lognormal distribution. As can be seen from Fig. 2, when SO_2 increases and during day a nucleation burst appears, SAM2 tends to bridge between the nucleation and the accumulation mode. During night, aerosols in nucleation sizes are not present and Aitken mode particles grow towards the accumulation mode (not shown). Thus the lowermost range of the predicted size distribution strongly varies depending on the availability of sunlight (here abstracted by the diurnal cycle in OH concentration). Consequently, in SAM2 the magnitude of the diurnal cycle in R_{eff} increases as the mass transfer rate onto the particles increases due to higher SO_2 mixing ratios. In SALSA, the mechanism to amplify the diurnal cycle in R_{eff} is similar to that of SAM2 but the coarse representation of the aerosol size distribution further increases the effect.

From the right column of Fig. 4 it can be seen that filtering the results in respect of an instruments lower detection limit at 0.05 µm, the predicted effective radii might evolve differently compared to the parameter when derived from the whole size range of the respective module. This characteristic is pronounced in lower stratospheric SO_2 concentrations, since the “signal-to-noise ratio” is much weaker than under volcanic

conditions. At the end of the simulation, for the lowest SO_2 concentrations shown in Fig. 4 the difference in R_{eff} relative to the parameter derived from the whole size range can reach 15% in the case of SALSA. Furthermore it can be seen that the formation of a diurnal cycle in the evolution of the effective radius is mainly caused by small particles. Whether the predicted size distributions in the nucleation and Aitken mode are affected by diurnal changes or not, it has an almost negligible effect on the filtered effective radii (as shown later, this does not apply to SALSA and SAM2 in the volcanic case).

It can be derived from Fig. 4 using miscellaneous integration ranges, that simply filtering model results with respect to observational data due to the definition of a certain cut-off size might lead to difficulties in the interpretation of the model results. Knowing and accounting for exact specifications, e.g. detection limits, of respective instruments are essential when predictions of aerosol size distributions are intended for such adaptations. Also, it is shown that the effective radius is very sensitive to the representation of particle growth in the modules, an effect which can also be shown in the validation of the global model MAECHAM5-SAM2 facing derived size parameters from several satellite retrievals and in situ measurements [Hommel et al., manuscript in preparation, 2009].

5.3.2 Low SO_2 concentration

The upper row of Fig. 4 shows the evolution of the effective radii as predicted by the modules under slightly increased stratospheric SO_2 mixing ratios. As shown in Fig. 2, in M7 setup 1 no clear bimodal distribution is predicted for SO_2=3.9×10^{-8} kg/kg, 900 s time step. When the effective radii are derived from the whole size range of M7, the calculated effective radii are almost overlapping in the mode setups 1 and 2. Also, M7 setup 3 gives qualitatively similar, but slightly lower values for the effective radius. Compared to MAIA, the modal module clearly overestimates the effective radius towards the end of the simulation by ~90%.

When the effective radius is calculated for the whole size range, SALSA reproduces fairly well the shape of the evolution of the effective radius, finally underestimating R_{eff} of MAIA in the mean by ∼20%.

SAM2 predicts very similar values as MAIA for the effective radius during night, but does not show a significant diurnal cycle. Under low concentrations of SO_2, SAM2 predicts a relatively smooth transition between the two modes. This results from numerical diffusion while solving the gas-to-particle partitioning with the hybrid advection scheme (see Hommel, 2008). At local extrema of the number distribution the growth of aerosols is solved by switching from an exponential solution of the equation of state to first order upwind scheme. This is accompanied by moderate numerical diffusion, resulting in a smaller diurnal cycle of the effective radius. Under higher concentrations of SO_2, the effect is reduced since either a distinct minimum in the number distribution is not predicted or a distinct gap in between the fine and the large mode is formed. In the latter case the hybrid scheme does not switch to upwind, so the diurnal cycle is represented in SAM2.

After setting the cut-off size of the effective radii is set to 0.05 µm (top right panel) and filtering the results, all modules show increasing effective radii in the beginning of the simulation before the evolution of this parameter decreases to a value which is approximately twice as high as when the whole particle size range is considered. Owing to its coarse particle size resolution, SALSA predicts a slightly increasing effective radius over about two third of the simulation, finally predicting a ∼15% higher R_{eff} as when derived from the whole modules size range. Also a finer resolution of the aerosol size range seems to better represent the effective radius using the sectional approach, since SAM2 follows most accurately the shape of its evolution as given by MAIA, even when the results are adapted to an optical instruments lower detection limit.

5.3.3 Moderate SO_2 concentration

When the initial SO_2 mixing ratio is increased to 3.9×10^{-6} kg/kg, compared to the reference model the setups 1 and 2 of M7 overestimate the effective radius for both

integration ranges. Since the aerosol is growing into a narrow mode of large particles as shown in Fig. 2, M7 setup 1 cannot reproduce the width of this mode, hence the effective radius is overestimated. Generally under the conditions here the representation of the effective radius in M7 benefit when no coarse mode is defined. In setup 1, the aerosols are grown to fairly large sizes much faster as in the setups 2 and 3. Compared to MAIA at the end of the simulation R_{eff} is overestimated by ~100% in setup 1 and ~40% in setup 2, while the evolution of R_{eff} in setup 3 almost accurately following those of the reference model.

Relative to the reference model here also SAM2 gives overall good results for the effective radius with almost overlapping results for the filtered parameter. Also SALSA performs qualitatively like under lower stratospheric SO_2 concentrations, but when the whole size range is considered in retrieving R_{eff}, the diurnal cycle is pronounced. At the end of the simulation, the relative difference in predicting R_{eff} compared to MAIA slightly increases to approximately 27% (mean of the last days diurnal cycle).

5.3.4 High SO_2 concentration

Under conditions we choose to be representative in the stratosphere after an injection of SO_2 from a large tropical volcanic eruption, the differences between the modules become distinct. When the global model time step length is used, the modules SALSA and SAM2 seem not be able to reproduce an effective radius as observed in the first month after e.g. the Mt. Pinatubo eruption in early summer 1991 (Russell et al., 1996; WMO/SPARC, 2006).

As shown in Fig. 2, the high concentration of gaseous sulphuric acid produced by SO_2 oxidation leading in time to the formation of a mode of large particles. The median radius of the mode is approximately a magnitude larger than the median radius of the large particle mode which appears under background conditions. Early in the simulation, in M7 setup 1 the aerosols grow rapidly into the coarse mode with σ_g=2.0, causing a general overestimation of the effective radius compared to the reference model MAIA (~40% at the end of simulation). With ~25% for M7 setup 2 the overestimation is lower

but significant, because as seen earlier in Sect. 3.1, M7 setup 2 better represents the very narrow mode of large particles as predicted by MAIA. Changing the standard deviation of the accumulation mode in M7 setup 3 to σ_g=1.2 and omitting the definition of a coarse mode leads to a pretty well reproduced evolution of R_{eff} compared to MAIA.

The coarse resolution of SALSA causes an inaccuracy in the calculated effective radius even though the shape of the size distribution matches well with the size distribution of MAIA (Fig. 2). Also, in Fig. 4 it can be seen that the assumption of fixed size sections in subregion 3 is not favorable under extreme volcanic conditions as the effective radius of particles larger than 0.05 µm reaches a constant value. Due to condensing sulphuric acid, new particles are quickly lost into large particles where the fixed size sections act only as a sink and thus prevent further growth of the particles.

Under assumed volcanic perturbations of the stratosphere, also SAM2 fails to represent the evolution of R_{eff}. Since in this module the particle growth due to condensation of H_2SO_4 is treated explicitly in time, the applied CFL criterion (e.g. Jacobson, 2005) limits the mass transfer from the gas to the particle phase for almost the whole size range defined in the module (particles are not allowed to grow beyond the size of their neighboring size section). Therefore, in the volcanic case, condensational growth is strongly underestimated in SAM2, leading to an asymptotic evolution of R_{eff}. The limitation of the mass flux onto the particles also accounts for the amplification in the diurnal cycle as well as for the formation of lower order oscillations preceding the increase in R_{eff} during the night time.

6 Conclusions

We have conducted an intercomparison of aerosol microphysics modules for use in the aerosol-climate model ECHAM5-HAM. We studied the evolution of an aerosol size distribution in an environment assumed to be representative in the stratosphere after the injection of SO_2 from modest to large volcanic eruptions.

It was found that the time increment used in the module integration can affect the

predicted shape of the aerosol distribution. These differences emphasize with increasing SO_2 mixing ratios. Whereas the definition of the mode structure in modal modules mainly account for this distinct different model behavior, it is thought that in sectional modules these differences are caused by the representation of aerosol-microphysical parameterizations. Although sectional modules designed for large scale applications are able to capture the evolution of a typical stratospheric background aerosol distribution to a narrowband bimodal structure in the volcanic case, they benefit from a higher resolution of the aerosol size range when the evolution of integrated aerosol size parameters is of particular interest, e.g. in climate process studies.

To further improve the ability of the modules to be used in global model studies of the climate impact from large volcanic eruptions, we have presented a new method for the integration of the time evolution equation for gas phase H_2SO_4 to be used in the ECHAM5-HAM microphysics module M7. The new time integration method outperforms the original M7 scheme as well as the Euler backward method when using the ordinary differential equation solver VODE as a reference. In M7 the fixed standard deviation was shown to be problematic when the size distribution is heavily modified by high concentrations of gaseous sulphuric acid. Then the assumption of σ_g=2 for the coarse mode results in a "tail" of too large particles which fall out of the stratosphere quicker than smaller coarse mode particles and which also might lead to an overestimation of the radiative response of a large volcanic eruption. This finding is extremely important for stratospheric aerosol modeling, because stratospheric sulfate particles are not deposited as quickly as in the troposphere and their lifetime is much longer. Therefore sedimentation becomes an important sink process, since the particle radius strongly determines the sedimentation velocity. A "tail" of too large particle would result in an unrealistically reduced lifetime of stratospheric sulfate aerosols.

A more general solution than the simple changing of the distribution σ_g of the log-normal distribution could be the development methods for alternating the standard deviation in different modes. This would nevertheless increase the number of prognostic variables, hence it degrades M7's computational benefits. The numerical treatment of

competing aerosol microphysical processes becomes important under high concentrations of SO_2 when the mass flux onto the particles is highest. Then other techniques than "classical" operator splitting and the explicit treatment of condensational growth can be favored as seen from improving the performance of the module M7 or even from the reference module MAIA.

Acknowledgements. The work contributed to the Super Volcano project at the Max-Planck Institute for Meteorology. H. Kokkola is supported by the Academy of Finland (project 119471). C. Timmreck is supported by the German Science Foundation DFG grant TI 344/1-1. J. Kazil is supported by the EC project EUCAARI. We would also like to thank Stefan Kinne for his helpful comments and Hanna Vehkamäki for providing an updated version of her nucleation parameterization.

The service charges for this open access publication
have been covered by the Max Planck Society.

References

Adams, P. J. and Seinfeld, J. H.: Predicting global aerosol size distributions in general circulation models, J. Geophys. Res.-Atmos., 107, 4–1, doi:10.1029/2001JD001010, 2002. 211

Brock, C., Jonsson, H., Wilson, J., Dye, J., Baumgardner, D., Borrmann, S., Pitts, M., Osborn, M., DeCoursey, R., and Woods, D.: Relationships between optical extinction, backscatter and aerosol surface and volume in the stratosphere following the eruption of Mt. Pinatubo, Geophys. Res. Lett., 22, 2555–2558, 1993. 212, 224

Brown, P. N., Byrne, G. D., and Hindmarsh, A. C.: VODE, A Variable- Coefficient ODE Solver, SIAM J. Sci. Stat. Comput., 10, 1038–1051, 1989. 215, 221

Chen, Y. and Penner, J. E.: Uncertainty analysis for estimates of the first indirect aerosol effect, Atmos. Chem. Phys., 5, 2935–2948, 2005, http://www.atmos-chem-phys.net/5/2935/2005/. 211

Chlond, A.: Locally modified version of Bott's advection scheme, Mon. Weather Rev., 122, 111–125, 1994. 218

Clegg, S. L., Rard, J. A., and Pitzer, K. S.: Thermodynamic properties of 0-6 mol kg^{-1} aqueous

sulfuric acid from 273.15 to 328.15 K, J. Chem. Soc., Faraday Trans., 90, 1875–1894, doi: 10.1039/FT9949001875, 1994. 215

Crutzen, P. J.: Albedo Enhancement by Stratospheric Sulfur Injections: A Contribution to Resolve a Policy Dilemma?, Climatic Change, 77, 211–220, doi:10.1007/s10584-006-9101-y, http://www.springerlink.com/content/t1vn75m458373h63, 2006. 212

Curtius, J., Froyd, K. D., and Lovejoy, E. R.: Cluster ion thermal decomposition (I): Experimental kinetics study and ab initio calculations for $HSO_4^-(H_2SO_4)_{(x)}(HNO_3)_{(y)}$, J. Phys. Chem. A, 105, 10 867–10 873, 2001. 215

Dubovik, O., Smirnov, A., Holben, B. N., King, M. D., Kaufman, Y. J., Eck, T. F., and Slutsker, I.: Accuracy assessments of aerosol optical properties retrieved from Aerosol Robotic Network (AERONET) Sun and sky radiance measurements, J. Geophys. Res., 105, 9791–9806, 2000. 227

Dusek, U., Frank, G. P., Hildebrandt, L., Curtius, J., Schneider, J., Walter, S., Chand, D., Drewnick, F., Hings, S., Jung, D., Borrmann, S., and Andreae, M. O.: Size Matters More Than Chemistry for Cloud-Nucleating Ability of Aerosol Particles, Science, 312, 1375–1378, doi: 10.1126/science.1125261, http://www.sciencemag.org/cgi/content/abstract/312/5778/1375, 2006. 211, 227

Fleming, J. R.: Historical Perspectives on Climate Change, Oxford University Press, New York, 1998. 210

Froyd, K. D. and Lovejoy, E. R.: Experimental Thermodynamics of Cluster Ions Composed of H_2SO_4 and H_2O. 1. Positive Ions, J. Phys. Chem. A, 107, 9800–9811, 2003a. 215

Froyd, K. D. and Lovejoy, E. R.: Experimental Thermodynamics of Cluster Ions Composed of H_2SO_4 and H_2O. 2. Measurements and ab Initio Structures of Negative Ions, J. Phys. Chem. A, 107, 9812–9824, 2003b. 215

Fuchs, N. A.: The Mechanics of Aerosols, Macmillan, 1964. 215

Gelbard, F., Tambour, Y., and Seinfeld, J. H.: Sectional representations for simulating aerosol dynamics, J. Colloid Interface Sci., 76, 541–556, 1980. 217

Ghan, S., Laulainen, N., Easter, R., Wagener, R., Nemesure, S., Chapman, E., Zhang, Y., and Leung, R.: Evaluation of aerosol direct radiative forcing in MIRAGE, J. Geophys. Res., 106, 5295–5316, 2001. 211

Ghan, S. J. and Schwartz, S. E.: Aerosol properties and processes: A path from field and laboratory measurements to global climate models, Bull. Am. Meteor. Soc., 88(7), 1059–1083, doi:10.1175/BAMS-88-7-1059, 2007. 212

Giauque, W. F., Hornung, E. W., Kunzler, J. E., and Rubin, T. T.: The thermodynamic properties of aqueous sulfuric acid solutions and hydrates from 15 to 300 K, Am. Chem. Soc. J., 82, 62–70, 1960. 215

Guo, S., Rose, W. I., Bluth, G. J. S., and Watson, I. M.: Particles in the great Pinatubo volcanic cloud of June 1991: The role of ice, Geochem. Geophy. Geosy., 5, Q05003, doi:10.1029/2003GC000655, 2004. 224

Hamill, P., Toon, O. B., and Kiang, C. S.: Microphysical processes affecting stratospheric aerosol particles, J. Atmos. Sci., 34, 1104–1119, 1977. 218

Hanson, D. R. and Lovejoy, E. R.: Measurement of the thermodynamics of the hydrated dimer and trimer of sulfuric acid, J. Phys. Chem. A, 110, 9525–9528, doi:10.1021/jp062844w, 2006. 215

Hommel, R.: Die Variabilität von stratosphärischem Hintergrund-Aerosol. Eine Untersuchung mit dem globalen sektionalen Aerosolmodell MAECHAM5-SAM2, Ph.D. thesis, Universität Hamburg, 2008. 211, 218, 231, 241

IPCC: Climate Change 2007: The scientific basis. Contribution of working group I to the fourth assessment report of the Intergovernmental Panel on Climate Change, Cambridge University Press, New York, 2007. 211

Jacobson, M. Z.: Developing, coupling and applying a gas, aerosol, transport and radiation model to study urban and regional air pollution, Ph.D. thesis, Dept. of Atmospheric Sciences, University of California, Los Angeles, 1994. 217

Jacobson, M. Z.: GATOR-GCMM: A global through urban scale air pollution and weather forecast model. 1. Model design and treatment of subgrid soil, vegetation, roads, rooftops, water, sea ice, and snow, J. Geophys. Res., 106, 5385–5402, 2001. 211

Jacobson, M. Z.: Fundamentals of Atmospheric Modeling, Second Edition, Cambridge University Press, New York, 2005. 216, 217, 233

Kazil, J. and Lovejoy, E. R.: A semi-analytical method for calculating rates of new sulfate aerosol formation from the gas phase, Atmos. Chem. Phys., 7, 3447–3459, 2007, http://www.atmos-chem-phys.net/7/3447/2007/. 221

Kazil, J., Lovejoy, E. R., Jensen, E. J., and Hanson, D. R.: Is aerosol formation in cirrus clouds possible?, Atmos. Chem. Phys., 7, 1407–1413, 2007, http://www.atmos-chem-phys.net/7/1407/2007/. 214, 241

Kerminen, V. M. and Kulmala, M.: Analytical formulae connecting the ”real” and the “apparent” nucleation rate and the nuclei number concentration for atmospheric nucleation events, J.

Aerosol Sci., 33, 609–622, 2002. 217
Kokkola, H., Korhonen, H., Lehtinen, K. E. J., Makkonen, R., Asmi, A., Järvenoja, S., Anttila, T., Partanen, A.-I., Kulmala, M., Järvinen, H., Laaksonen, A., and Kerminen, V.-M.: SALSA – a Sectional Aerosol module for Large Scale Applications, Atmos. Chem. Phys., 8, 2469–2483, 2008,
http://www.atmos-chem-phys.net/8/2469/2008/. 211, 217, 241
Lauer, A., Hendricks, J., Ackermann, I., Schell, B., Hass, H., and Metzger, S.: Simulating aerosol microphysics with the ECHAM/MADE GCM – Part I: Model description and comparison with observations, Atmos. Chem. Phys., 5, 3251–3276, 2005,
http://www.atmos-chem-phys.net/5/3251/2005/. 211
Le Treut, H., Somerville, R., Cubasch, U., Ding, Y., Mauritzen, C., Mokssit, A., Peterson, T., and Prather, M.: Climate Change 2007: The Physical Science Basis, Contribution of Working Group I to the Fourth Assessment Report of the Intergovernmental Panel on Climate Change, edited by: Solomon, S., Qin, D., Manning, M., Chen, Z., Marquis, M., Averyt, K. B., Tignor, M., and Miller, H. L., chap. Historical Overview of Climate Change, Cambridge University Press, Cambridge, United Kingdom and New York, NY, USA, 2007. 210
Liao, H. and Seinfeld, J.: Global impacts of gas-phase chemistry-aerosol interactions on direct radiative forcing by anthropogenic aerosols and ozone, J. Geophys. Res., 110, D18208, doi:10.1029/2005JD005907, 2005. 211
Liu, H. Q., Pinker, R. T., and Holben, B. N.: A global view of aerosols from merged transport models, satellite, and ground observations, J. Geophys. Res., 110, D10S15, doi:10.1029/2004JD004695, 2005. 211
Lovejoy, E. R. and Curtius, J.: Cluster ion thermal decomposition (II): Master equation modeling in the low pressure limit and fall-off regions. Bond energies for $HSO_4^-(H_2SO_4)_x(HNO_3)_y$, J. Phys. Chem. A, 105, 10874–10883, 2001. 215
Lovejoy, E. R., Curtius, J., and Froyd, K. D.: Atmospheric ion-induced nucleation of sulfuric acid and water, J. Geophys. Res., 109, D08204, doi:10.1029/2003JD004460, 2004. 214, 241
Rasch, P. J., Crutzen, P. J., and Coleman, D. B.: Exploring the geoengineering of climate using stratospheric sulfate aerosols: The role of particle size, Geophys. Res. Lett., 35, 2809, doi:10.1029/2007GL032179, 2008. 211
Rasch, P. J., Tilmes, S., Turco, R. P., Robock, A., Oman, L., Chen, C.-C., Stenchikov, G. L., and Garcia, R. R.: An overview of geoengineering of climate using stratospheric sulfate aerosols, Phil. Trans. Royal Soc. A, doi:10.1098/rsta.2008.0131, 2008. 212

Read, W. G., Froidevaux, L., and Waters, J. W.: Microwave limb sounder measurement of stratospheric SO_2 from the Mount Pinatubo volcano, Geophys. Res. Lett., 20, 1299–1302, 1993. 222

Reddy, M. S., Boucher, O., Bellouin, N., Schulz, M., Balkanski, Y., Dufresne, J. L., and Pham, M.: Estimates of global multicomponent aerosol optical depth and direct radiative perturbation in the Laboratoire de Meteorologie Dynamique general circulation model, J. Geophys. Res., 110(D10), D10S16, doi:10.1029/2004JD004757, 2005. 211

Rodriguez, M. and Dabdub, D. J.: IMAGES-SCAPE2: A modeling study of size and chemically resolved aerosol thermodynamics in a global chemical transport model, J. Geophys. Res., 109, D02203, doi:10.1029/2003JD003639, 2004. 211

Roeckner, E., Bäuml, G., Bonaventura, L., Brokopf, R., Esch, M., Giorgetta, M., Hagemann, S., Kirchner, I., Kornblueh, L., Manzini, E., Rhodin, A., Schlese, U., Schulzweida, U., and Tompkins, A.: The atmospheric general circulation model ECHAM5. PART I: Model description, MPI-Report, 349, 127 pp., 2003. 214

Russell, P. B., Livingston, J. M., Pueschel, R. F., Bauman, J. J., Pollack, J. B., Brooks, S. L., Hamill, P., Thomason, L. W., Stowe, L. L., Deshler, T., Dutton, E. G., and Bergstrom, R. W.: Global to microscale evolution of the Pinatubo volcanic aerosol, derived from diverse measurements and analyses, J. Geophys. Res., 101, 18745–18763, 1996. 212, 232

Seinfeld, J. H. and Pandis, S. N.: Atmospheric Chemistry and Physics, John Wiley & Sons Inc., 1998. 211

Spalding, D. B.: A novel finite–difference formulation for differential expressions involving both first and second derivatives, Int. J. Num. Methods, 4, 551–559, 1972. 218

Spracklen, D. V., Pringle, K. J., Carslaw, K. S., Chipperfield, M. P., and Mann, G. W.: A global off-line model of size-resolved aerosol microphysics: II. Identification of key uncertainties, Atmos. Chem. Phys., 5, 3233–3250, 2005, http://www.atmos-chem-phys.net/5/3233/2005/. 211

Stier, P., Feichter, J., Kinne, S., Kloster, S., Vignati, E., Wilson, J., Ganzeveld, L., Tegen, I., Werner, M., Balkanski, Y., Schulz, M., Boucher, O., Minikin, A., and Petzold, A.: The aerosol-climate model ECHAM5-HAM, Atmos. Chem. Phys., 5, 1125–1156, 2005, http://www.atmos-chem-phys.net/5/1125/2005/. 211, 215, 241

Thomason, L. W., Burton, S. P., Luo, B.-P., and Peter, T.: SAGE II measurements of stratospheric aerosol properties at non-volcanic levels, Atmos. Chem. Phys., 8, 983–995, 2008, http://www.atmos-chem-phys.net/8/983/2008/. 227

Timmreck, C.: Three-dimensional simulation of stratospheric background aerosol: First results of a multiannual GCM simulation, J. Geophys. Res., 106, 28313–28332, 2001. 211

Timmreck, C. and Graf, H.-F.: A microphysical model to simulate the development of stratospheric aerosol in a GCM, Meteorol. Zeitschr., 9, 263–282, 2000. 218, 241

Timmreck, C., Graf, H.-F., and Steil, B.: vol. 139, chap. Aerosol chemistry interactions after the Mt. Pinatubo eruption, AGU Monograph, 139, 214–225, 2003. 222

Twomey, S.: Pollution and the planetary albedo, Atmos. Environ., 8, 1251–1256, 1974. 211

Vehkamäki, H., Kulmala, M., Napari, I., Lehtinen, K. E. J., Timmreck, C., Noppel, M., and Laaksonen, A.: An improved parameterization for sulfuric acid-water nucleation rates for tropospheric and stratospheric conditions, J. Geophys. Res., 107(D22), AAC3.1–AAC3.10, doi:10.1029/2002JD002184, 2002. 214, 217

Vignati, E., Wilson, J., and Stier, P.: M7: An efficient size-resolved aerosol microphysics module for large-scale aerosol transport models, J. Geophys. Res., 109, D22202, doi:10.1029/2003JD004485, 2004. 211, 215, 216, 241

Weart, S.: The Discovery of Global Warming, Harvard University Press, Cambridge, MA, 2003. 210

Wilson, J. and Raes, F.: M3 a multi modal model for aerosol dynamics, Proceedings of the 14th International Conference on Nucleation and Atmospheric Aerosols, 458–461, 1996. 223

Wilson, J., Cuvelier, C., and Raes, F.: A modeling study of global mixed aerosol fields, J. Geophys. Res., 106, 34081–34108, 2001. 211, 223

WMO/SPARC: WMO/SPARC Scientific Assessment of Stratospheric Aerosol Properties (ASAP), Tech. rep., 2006. 212, 222, 232

Zhang, Y., Easter, R. C., Ghan, S. J., and Abdul-Razzak, H.: Impact of aerosol size representation on modeling aerosol-cloud interactions, J. Geophys. Res., 107, 4558, doi:10.1029/2001JD001549, 2002. 211

Table 1. Major characteristics of M7, SALSA, SAM2, and MAIA.

	M7	SALSA	SAM2	MAIA
Method for describing the size distribution	modal	sectional, moving center + fixed center for three largest size sections	sectional, fixed center	hybrid kinetic-sectional, fixed center, first order approximation of size distribution inside geometric size sections
Number of modes or size sections	7	20 (10 in size space)	44	21 kinetic, 99 geometric
Chemical species treated	sulphate, organic carbon, mineral dust, sea salt	sulphate, organic carbon, mineral dust, sea salt	sulphate	sulphate
References	Vignati et al. (2004) Stier et al. (2005)	Kokkola et al. (2008)	Hommel (2008) Timmreck and Graf, 2000	Lovejoy et al. (2004) Kazil et al. (2007)

Table 2. Ambient parameters and the initial values for the the production rate of gas phase sulphuric acid, the pre-existing aerosol size distribution, and sulphuric acid gas phase concentration for the evaluation of the new time integration scheme for three different test cases.

	case 1	case 2	case 3
Temperature (K)	255	225	285
RH (%)	80	50	90
production rate ($cm^{-3}\,s^{-1}$)	100 000	10 000	50 000
condensation sink (s^{-1})	0.001	0.0001	0.01
Initial [H_2SO_4] (cm^{-3})	1×10^{6}	7.5×10^{7}	1×10^{8}

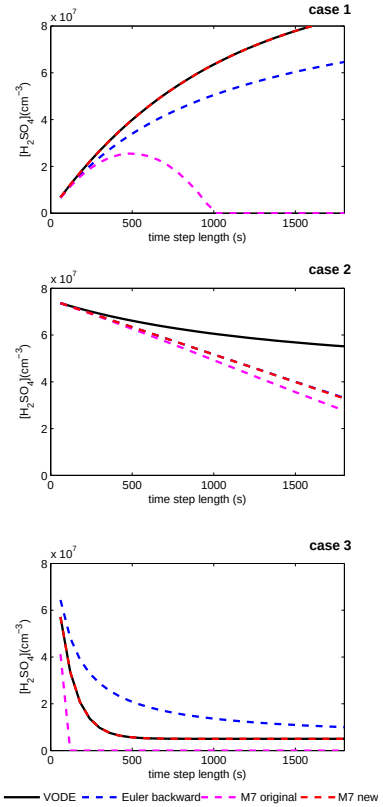

Fig. 1. Gas phase concentration of sulphuric acid after one time step, calculated with the Euler backward scheme, the original M7 operator splitting method, and the new time integration method. As a reference, the gas phase sulphuric acid concentration calculated with the VODE solver is given. In this case, the abscissa denotes the integration time, which is divided into shorter time steps by VODE according to a desired relative error tolerance.

GMDD
2, 209–246, 2009

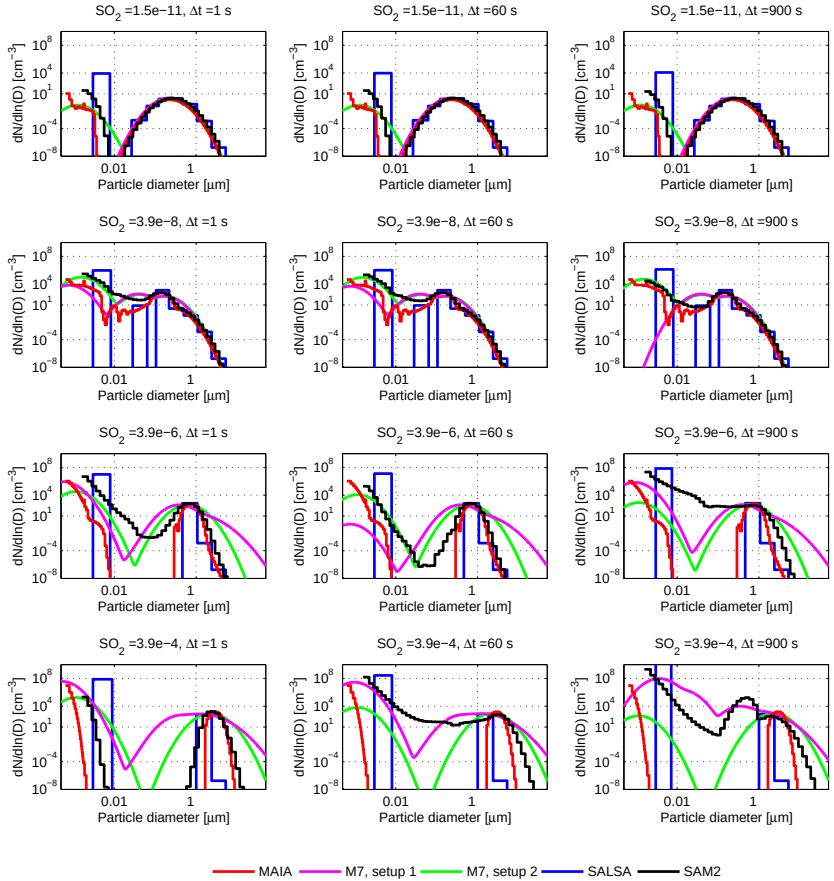

Fig. 2. Aerosol number size distributions at noon of the 10th day of the simulations calculated using different aerosol microphysics modules and the reference model. The size distributions were calculated for four different initial gas phase SO_2 mixing ratios and three different time step lengths Δt. The SO_2 mixing ratios (kg kg^{-1}) and time step lengths are given on the title of each sub-figure.

GMDD
2, 209–246, 2009

Title Page
Abstract Introduction
Conclusions References
Tables Figures
◀I ▶I
◀ ▶
Back Close
Full Screen / Esc
Printer-friendly Version
Interactive Discussion

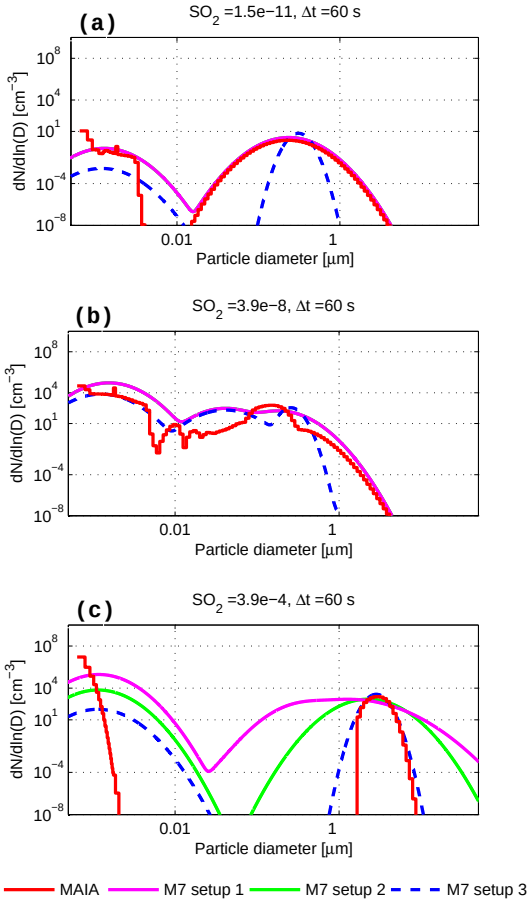

Fig. 3. The aerosol number size distribution at noon of the 10th day of the simulation calculated using the reference model MAIA and M7 with three different different mode setups for different initial SO_2 concentrations: **(a)** 1.5×10^{-11} kg/kg, **(b)** 3.9×10^{-8} kg/kg, and **(c)** 3.9×10^{-4} kg/kg.

GMDD
2, 209–246, 2009

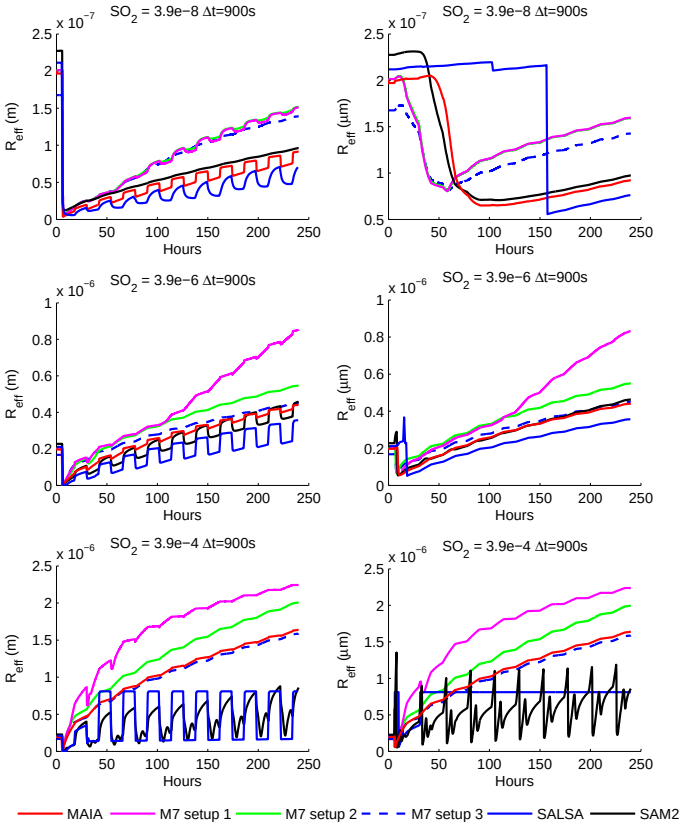

Fig. 4. Evolution of the effective radius for the modules MAIA, SALSA, SAM2, and M7 in three mode setups, using three different SO_2 mixing ratios (kg kg^{-1}). In the left column R_{eff} is derived for the whole aerosol size range as defined by the modules, in the right column the integration range starts at 0.05 µm.